



Stretched 1000-L microbial fuel cell

Maxime Blatter^a, Louis Delabays^b, Clément Furrer^a, Gérald Huguenin^b,
Christian Pierre Cachelin^d, Fabian Fischer^{a,c,*}

^a Institute of Life Technologies, HES-SO Valais-Wallis, Route du Rawyl 64, Sion, CH-1950, Switzerland

^b Embedded-Computing Systems, Haute-Ecole Arc, Rue de la Serre 7, St-Imier, CH-2610, Switzerland

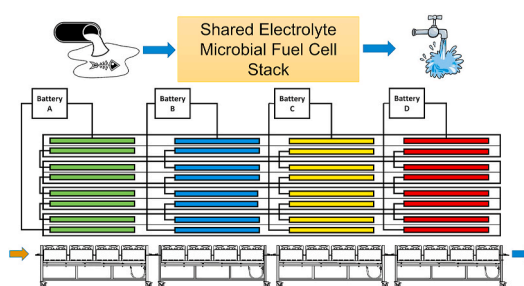
^c Institute of Sustainable Energy, HES-SO Valais-Wallis, Route du Rawyl 47, CH-1950, Switzerland

^d Institute of Systems Engineering, HES-SO Valais-Wallis, Route du Rawyl 47, CH-1950, Switzerland

HIGHLIGHTS

- 1000 L Shared electrolyte microbial fuel cell showing no electrical interferences.
- Energy efficiency was highest so far for municipal wastewater microbial fuel cell.
- Maximum power point tracking optimized power generation and COD removal.
- Metagenomics showed that top 10 genera cleaned wastewater and generated power.
- It worked all-seasons, from 11.5 to 21 °C and voltage reversals were self-healing.

GRAPHICAL ABSTRACT



ARTICLE INFO

Keywords:

Bioelectricity
Scale-up
Metabolism
Wastewater
Tracking
Metagenomics

ABSTRACT

The construction of large microbial fuel cells (MFCs) and their long-term reliability are current challenges. MFCs generate power while purifying wastewater, save electricity, avoid pollutant stripping into the air and are a source of CO₂. To understand larger MFCs, a 1000-L MFC was designed. It was built from transparent polyester and electrodes were from reticulated vitreous carbon. Four power management devices were connected to an ensemble of 64 MFC units and assembled as a 12 m long MFC. Two Raspberry and a personal computer with Python programmed software automatized power management. The MFC was run for one year under maximum power point tracking (MPPT). Temperatures between 11.5 °C and 21 °C corresponded to WWTP conditions. The reactor shared electrolytes within 12 m long half-cells and 80–95% COD was removed generating 0.015 to 0.060 kWh/m³ with an energy efficiency of 5.8–12.1%. Voltage reversal were seen as potential imbalances among MFC units and all self-healing. Ammonium removal reached 48%, phosphorous was reduced to 0.59 mg/L, and micropollutants degraded by 67%. Biofilm mapping by 16S rRNA metagenomics indicated bi-sectorial metabolic properties. 10 Major genera were essential in the elongated scale up MFC generating electricity, reduced energy needed, and purified wastewater.

* Corresponding author. Institute of Life Technologies, HES-SO Valais-Wallis, Route du Rawyl 64, CH-1950, Switzerland.

E-mail addresses: fabian.fischer@hevs.ch, fabian.fischer@hevs.ch (F. Fischer).

<https://doi.org/10.1016/j.jpowsour.2020.229130>

Received 21 August 2020; Received in revised form 12 October 2020; Accepted 26 October 2020

Available online 7 November 2020

0378-7753/© 2020 The Authors.

Published by Elsevier B.V. This is an open access article under the CC BY-NC-ND license

(<http://creativecommons.org/licenses/by-nc-nd/4.0/>).

1. Introduction

Wastewater treatment consumes 1–2% of electricity in industrialized countries [1]. This notable energy consumption is due to highly powered air pumps that saturate influent wastewater with air-oxygen. This procedure ensures efficient microbial respiration and accelerates waste digestion. The process consumes ~70% of electricity needed to operate a municipal wastewater treatment plant (WWTP) [2–4]. Conversely, there is considerable energy contained in wastewater (1.9 kWh/m³) [5]. This is in most WWTPs more energy than needed for treatment (0.3–2.1 kWh/m³) [6,7].

Bioelectric wastewater treatment potentially will invert today's power consumption into tomorrow's energy generation. The microbial fuel cell (MFC) based purification process is performed with electrogenic and other anaerobic microorganisms. Electrogenic microbes respire over anodes and generate electricity while digesting waste. The power recoveries so far achieved were between 0.015 and 0.024 kWh/m³ [8,9]. The recoverable energy for a WWTP of 100'000 people equivalents corresponds to the electricity consumption of 42–67 households (5200 kWh/y per home). Even higher are energy savings due to much reduced aeration, what corresponds to another 100 household equivalents when based on a 75% reduced energy consumption with dual chambered MFCs and compared to lagoon aeration.

The use of MFCs as power generators is particularly challenging when wastewater becomes almost clean. There, power generation drops due to fuel starvation effects and mass transfer limitations and removing residual COD is sluggish.

Another useful purification process in wastewater MFCs is ammonia transformation into nitrite and nitrate, which is subsequently reduced into nitrogen [10]. This redox process is initially electron producing and then consuming and not adding to the power generation faculty of wastewater MFCs [11]. Beside this, ammonia is eventually recoverable from the cathode as it migrates through the cation exchange membrane. However, ammonia migration is not a major process and competes with other cations such as: H⁺, Na⁺, K⁺, Mg²⁺ and Ca²⁺ [12].

The above discussed capacity of MFCs to purify wastewater was shown for litre scale reactors [8]. Large-scale microbial fuel cells with energy harvesting electronics, more than 100 L, are not widely documented [13]. With larger setups mixed performance results are reported and most problematic were power generation problems after several weeks of operation. This is at an early stage and a serious problem for the prospect of MFC driven wastewater treatment, as it should work for decades [14]. There are many processes in a MFC that require control. If one of them is deteriorating, a rapid resolution is needed to perform the purification process over a prolonged time. Wastewater is not an all convenient substrate in contrast to others that would lower the risk of MFC failure. These are: synthetic mixtures, urine, and wastewater from food processing [15].

Another complication with stacked MFCs for enhanced performance, are voltage reversals. They are caused often by fuel starvation [16], other reasons are high stack currents [17] and internal resistances rise resulting in voltage reversals of individual MFC units in the stack and failure from microbial stress [18]. Another reason were corrosive effects by damaged electrodes destroying biofilms [19]. In addition, small changes in individual MFC units result in imbalances among MFC units and reversals occur just as voltage sweeps for this reason [20].

Amid all technical inconveniences the concept is attractive for treating municipal wastewater, as it is a cheap and most abundant feed stock. To achieve process robustness, considerable scientific challenges remain, in generating efficiently electricity from microbes. The working potential of an MFC is 0.5 V under ideal conditions and a serial stack of four MFCs generates 2.0 V [21]. This potential is high enough to transform obtained power into useful electricity. The difficulty with electricity generation in wastewater treatment-MFCs is power decline due to COD removal as wastewater becomes purified [22]. Therefore, low voltages and currents need to be considered too. The question is how

to choose an appropriate design for scale up MFCs to ensure its function at all conditions, structural stability and best performance.

Structural stability of larger microbial fuel cells was studied recently with the construction of three 168-L microbial electrolysis cells used equally as MFCs [23]. They consisted of a 2.4 m long common anode chamber and an external steel frame for structure reinforcement. These reactors remained functional for at least two years in WWTPs. The building of bioelectric systems reactors longer than 2.4 m were challenging for constructors. This because longer than 2.4 m stiff polymer plates were not available and automatized cutting tools were neither laid out for larger plates and manual work would be needed enhancing construction cost. To solve this problem, multiple smaller reactors could be built by more automatized construction steps resulting in series of hyphenated small reactors. However, WWTPs deals with large volumes and bigger sized units decrease the numbers for needed fittings, cables, tubes and sensors.

In this work a 1000-L MFC was planned by computer aided design (CAD), constructed, and operated. The 12 m long MFC-reactor was installed in an underground gallery of a municipal WWTP (Château neuf, Switzerland). The temperature of the MFC-reactor was roughly identical to the one in aerated lagoons just above the 1000-L MFC. Examined parameters were chemical oxygen demand (COD), power, energy efficiency (EE), Coulomb efficiency (CE), pH, internal resistances, voltage reversals, nitrification, denitrification, desulfurisation, phosphate reduction and micropollutant removal. Energy generation was optimized by maximum power point tracking (MPPT) and electricity stored on lithium batteries. 64 Anodic microbiomes were sequenced for structure and metabolic mapping using 16S rRNA method.

2. Materials and methods

2.1. Microbial fuel cell construction and installation

A common electrolyte dual chambered microbial fuel cell architecture was chosen to run the setup with an aqueous cathode. The aqueous cathode was preferred as the tin and tissue like membranes were not exposed to liquid pressure and related bending. Secondly, O₂ concentrations were adjustable avoiding uncontrollable diffusion into anodes. Another feature was the common electrolyte MFC approach reducing the complexity of the stack to eight electrolyte channels/half cells [21]. The electrolytes were pumped by two four-channel pumps into the 12 m long half cells (simulated gravity flux) (Fig. 1A). The entire 1000-L MFC was assembled from 64 MFC units, which were physically and electronically organized into four quadruple MFC-sub-stacks (Fig. 1B). Each MFC-sub-stack was independent in terms of electronic circuits and related power management as well as electricity harvest. These four power tracking and storage units were connected to two Raspberry Pi computers, which were then connected to a personal computer connected to the internet.

The 1000-L MFC construction plan was established by CAD (Inventor software). The reactor was built by the polymechanic shop of HES-SO Sion. It consisted of 64 MFC units of 16.25 L each made from polyethylene terephthalate glycol (PETG) (67.0 × 46.4 × 14.1 cm). The liquid volume of the MFC was 928–1034 L. VANADion membranes (Ion Power) divided half-cells into equitable volumes. Eight reticulated vitreous carbon (RVC) electrodes (21 × 13 × 3 cm) were fixed per MFC unit. 16 MFC units were assembled per 3 m long and 46 cm wide carts representing each a MFC-sub-stack. Four of such carts were interconnected to a linear MFC train of >12 m length (stretched MFC = total setup ~14 m long, 61 cm wide, 1.9 m high). This established eight common electrolyte MFC channels passing through four MFC-sub-stacks (common electrolyte MFC stack concept [24]). The 1000-L MFC was operated as four quadruple stacks with flow through wastewater treatment (Fig. 1B). Wastewater and catholyte were supplied by two 4-channel peristaltic pumps (BT100S-1, Golander Pump). The catholyte was from a groundwater table spring on the WWTP's site containing 0.0–0.7

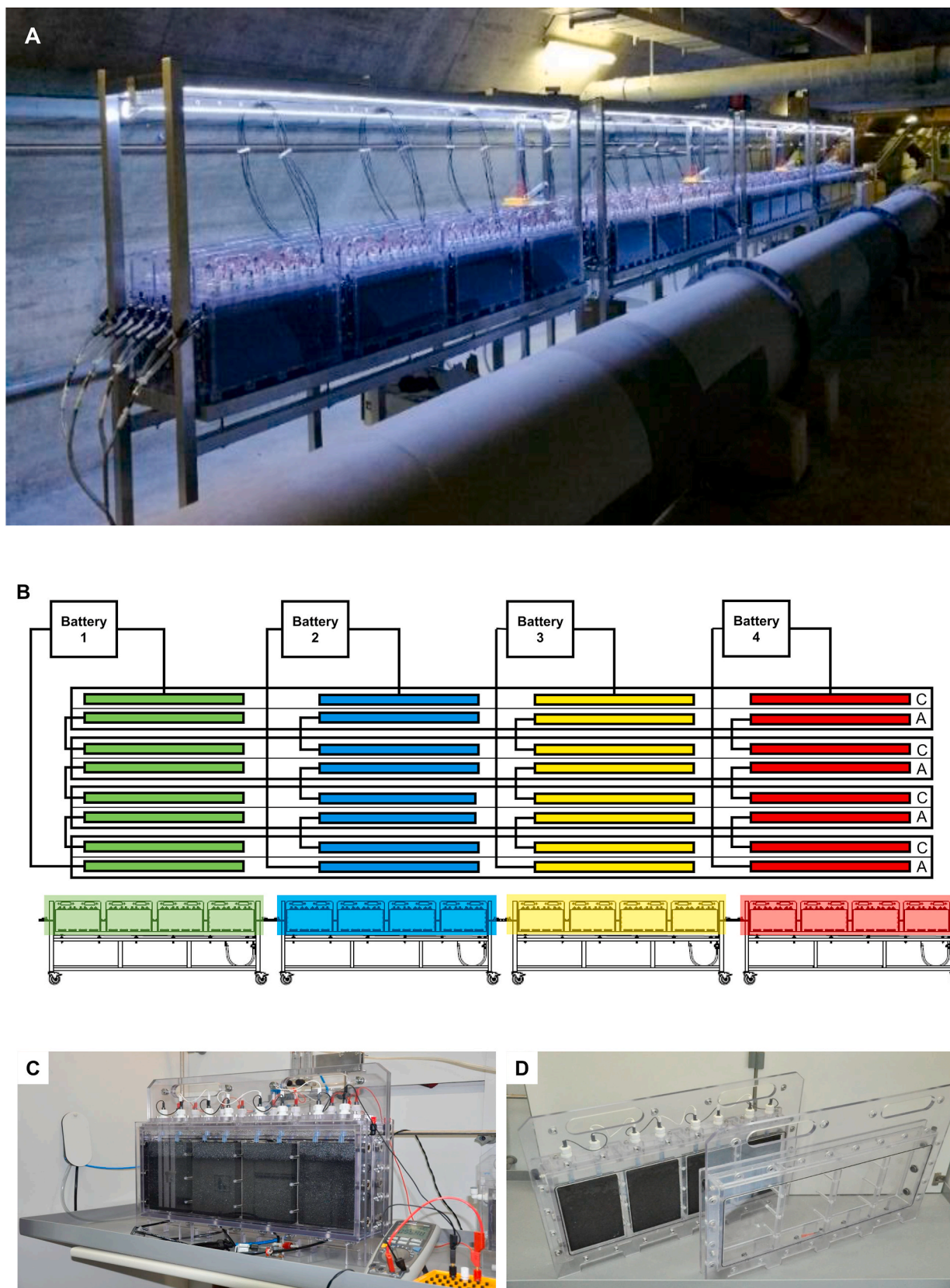


Fig. 1. A) Stretched 1000-L MFC stack in an underground gallery below aerated lagoons in WWTP Chateauneuf. B) Shared common electrolytes (A = anode is wastewater, C = cathode is groundwater) in 12 m long “channels”. The 1000-L MFC was organized into four MFC-sub-stacks: green, blue, yellow and red electrodes. Each MFC-sub-stack was a serial stack of four MFCs, assembled from $4 \times 4 = 16$ MFC units. Wastewater flew from left to right passing all MFC-sub-stacks. C) MFC unit, one out of 64. D) Two MFC half cells with RVC electrodes (in the back) and construction details (in front). (For interpretation of the references to colour in this figure legend, the reader is referred to the Web version of this article.)

mg/L of O₂. The wastewater was from the WWTP's primary clarifier, cleared from particles and oily substances. Air was bubbled over a central tube (0.5 bar, 0.5 L/s) into all 64 MFC cathodes using polyamide tubes (PA, 4 mm ID) and dosage clamps (~8 mL/s of air per MFC unit).

Power harvest was organized for each cart/MFC-sub-stack individually by an electronic power management board. Each MFC-sub-stack (16 MFC units) was a serial MFC stack of four MFCs (Fig. 1B). A single MFC consisted therefore of a linear series of 4 MFC units with a total volume of 62.5 L adding up to 250-L per MFC-sub-stack.

For the installation, prefabricated parts, fittings and other equipment were transported to the WWTP (Château-neuf, Switzerland), where the MFC was assembled. The reactor was placed in an underground gallery, just below the aerated lagoons (Fig. 1A). The gallery's temperature corresponded to wastewater temperature throughout all seasons allowing to compare MFC purification performance to state of the art wastewater treatment in the lagoons. The MFC was acclimatized with an external resistance of 1000 Ohm under a constant wastewater flux 20 L/h and groundwater as catholyte at 10 L/h. Biofilms grew on the RVC anodes in a self-organized manner what lasted several weeks, and best biofilms were grown after 5–6 months.

2.2. Oxygen, pH and temperature measurements

Electrolyte samples were taken from connection tubes in-between MFC-carts. O₂ concentrations and temperature were recorded with an oxygen probe (HI2040 edge, Hanna Instruments). The pH was determined with a standard pH electrode (827 pH lab, Metrohm). The three parameter recording lasted 100 min for the entire 1000-L MFC.

2.3. Electronic circuit management, power tracking, electricity harvest and storage

To monitor all 64 MFC units of the 1000-L MFC, a corresponding number of electronic boards were manufactured to interlink all MFC units with a Raspberry Pi B3 microcomputer. It exchanged data with a central personal computer connected to the internet. Needed software was programmed with Python language. The electronic management setup was divided into four MFC-sub-stacks; which organized unit and stack electricity such as currents, voltages and powers. Power generation was optimized by maximum power point tracking (MPPT), harvested and stored on lithium batteries (Li - Mn 3.7 V/2250 mAh, Sony). The four power tracking and storage units were managed by a second Raspberry Pi B3 microcomputer, equally connected with the central computer. All electronic circuit management and other devices were operated with grid power as the system was not designed to be self-sufficient.

2.4. Chemical oxygen demand and Coulomb efficiency

Chemical oxygen demand (COD) was determined with Nanocolor® tube tests (ISO 15705:2002). COD removal effectiveness (ϵ_{COD} [%]) (Eq. (2)) was calculated from the inlet values to 1000-L MFC (COD_{in} [mg O₂/L]) and outlet ports COD_{out} [mg O₂/L]:

$$\epsilon_{COD} = \frac{COD_{in} - COD_{out}}{COD_{in}} \cdot 100 \quad (2)$$

Coulombic Efficiencies (CE) were electrons (Coulomb) transferred by the anode and maximum COD possible [25]. Parasite oxidation for biomass formation, competitive reactions and organic mass sedimentation were not deduced due to the lack of a precise mass balance for the entire process [26]. The CE (ϵ_{Cb} [%]) was calculated slightly different for batch (Eq. (3)) and continuous processing (Eq. (4)):

$$\epsilon_{Cb} = \frac{M \int_0^t I dt}{F b \nu_{An} \Delta COD} \cdot 100 \quad (3)$$

or

$$\epsilon_{Cb} = \frac{M I}{F b q_{An} \Delta COD} \cdot 100 \quad (4)$$

$M = 32$ [g/mol]: MW of O₂, $F = 96485$ [C/mol]: Faraday constant, $b = 4$ [-]: number of electrons exchanged per mole oxygen, I [A]: current generated by MFC, ΔCOD [mg O₂/L]: COD change over time (Eq. (3)) or difference between influent and effluent COD (Eq. (4)), t [s]: process time, ν_{An} [m³]: anolyte volume and q_{An} [m³/s]: anolyte flow rate.

2.5. Normalized energy recovery

Normalized Energy Recovery (NER) was calculated as kWh to assess the performance of the wastewater MFC process. The kWh unit is more convenient to discuss the MFC's potential in wastewater treatment (WWT) than power per electrode (surface, volume) to compare MFC performance. Normalized energy recovery (NER) per wastewater volume was therefore considered to assess MFC power output of the 1000-L MFC in continuous processing [27,28]. The NER was calculated by Eq. (5) (NER_V [kWh/m³]) and COD removal NER_{COD} [kWh/kg COD] Eq. (6).

$$NER_V = \frac{\int_0^t P dt}{\nu_{An}} = \frac{\bar{P}}{q_{An}} \quad (5)$$

and

$$NER_{COD} = \frac{NER_V}{\Delta COD} \quad (6)$$

P [kW]: power of MFC (\bar{P} average power), t [h]: process time, ν_{An} [m³]: anolyte volume, q_{An} [m³/h]: anolyte flow rate and ΔCOD [g O₂/m³]: COD change with time or difference between influent and effluent CODs.

By comparing generated energy per kilogram of COD in wastewater with the theoretical maximal recoverable energy of 3.86 kWh/kg COD [5,29] the energy efficiency (EE) was calculated ϵ_{En} [%] (Eq. (7)).

$$\epsilon_{En} = \frac{NER_{COD}}{3.86 \frac{kWh}{kg COD}} \cdot 100 \quad (7)$$

2.6. Metagenomics

Microbiomes on electrodes were analysed by the 16S rRNA V4–V5 method. Biofilm samples were cut from RVC electrodes in a quasi-quantitative manner. Small disks (ID = 8 mm) with surficial biofilms ($S = 0.5$ cm²) were cut out from anode sides vicinal to CE-membranes. Two samples (disks) were cut from the opposite corners per electrode and then combined for extraction. In total, 128 anodic and 16 cathodic samples were taken, and DNA was extracted using "FastDNA™ SPIN Kit for Soil" (MP Biomedicals). Extracted DNA in combined samples (64 and 8) were quantified with Qubit™ dsDNA HS Assay Kit (Invitrogen) to ensure > 1 ng/μl of DNA for amplification and sequencing. The 16S rRNA V4–V5 analysis of the samples was performed by the IMR centre for comparative genomics and evolutionary bioinformatics (Dalhousie University, Canada).

3. Results and discussion

3.1. Long common electrolyte microbial fuel cell: structure and process design rational

The common electrolyte design was newly and successfully applied on the 1000-L MFC scale. Small scale common electrolyte MFCs are sometimes difficult to manage [21]. The hypothesis was, that in a long poly stack architecture with constant electrolyte flow, ionic cross conduction is avoided and no interferences should be observed. This assumption was largely fulfilled. Shared common electrolytes simplified MFC power generation and wastewater purification, without the need of

multiple pumping stations in between MFC units. The 1000-L MFC was run in this manner for 18 months with municipal wastewater without significant down times. After initial 5–6 months of acclimatisation best powers were reached (Fig. 2B). From this moment on, the MFC reactor was run for ~400 days with four MPPTs. The energy was harvested from four quadruple MFC-sub-stacks sharing all the same electrolytes (wastewater as anolyte and groundwater as catholyte) (Fig. 1B). In such a multiple unit MFC many electronic interconnections were possible. To keep construction cost low a relatively simple electronic setup was chosen. With this equipment the 1000-L MFC was so far the longest ever constructed common electrolyte reactor, combined with MPPT and power storage. It enabled plenty of novel insights at this larger scale.

3.2. Acclimatisation until reaching maximum power

The acclimatisation of the 1000-L MFC was performed under constant wastewater flux against a 1000 Ohm resistance. The anodes and cathodes were used without chemical pre-treatment or catalyst deposition. Biofilms developed on anodes in a self-organized manner from microbes contained in wastewater. Acclimatisation progress was weekly examined by polarisation experiments which showed increasing P_{max} values for four months at 1000 Ohm (Fig. 2B). The acclimatisation with 1000 Ohm resistances was a prudent approach developed earlier [18]. The highest internal resistances reached 67 Ohm and was as low as 14.1 Ohm in the best case during this period (Fig. 2C). However, when a

problem occurred the internal resistance rose in one case to 850 Ohm what could change properties very much by current inversion and therefore a static 1000 Ohm resistance was justified in a manually controlled setting. To overcome such problems automatized P_{max} control was the other solution. With the fourth month, maximum power point tracking electronics was installed what accelerated biofilm growth and power performance reached an all-time maximum two months later (Fig. 5B). In this best power generation situation the internal resistance was the lowest with 14.1–19.9 Ohm. Beside this, it is noteworthy that the acclimatisation was performed from fall into winter season with declining temperatures of 1–2 °C per month (Fig. 5C).

After best powers were reached, they began to decline as observed from data recorded under continuous processing using MPPT (Fig. 3). Conversely, manually recorded polarisation data showed maximum power values that remained stable for the same four months although the MFC was operated with slightly declining COD concentrations (Fig. 5B). This COD dilution was attributed to more frequent rainfalls in the spring and summer seasons (Fig. 5A). Probably, the manual polarisation experiment allowed biofilms to recharge before recordings were performed (Fig. 3). Moreover, manual polarisations were performed during weekdays under ideal conditions, rainy days were avoided and sediment accumulations resolved.

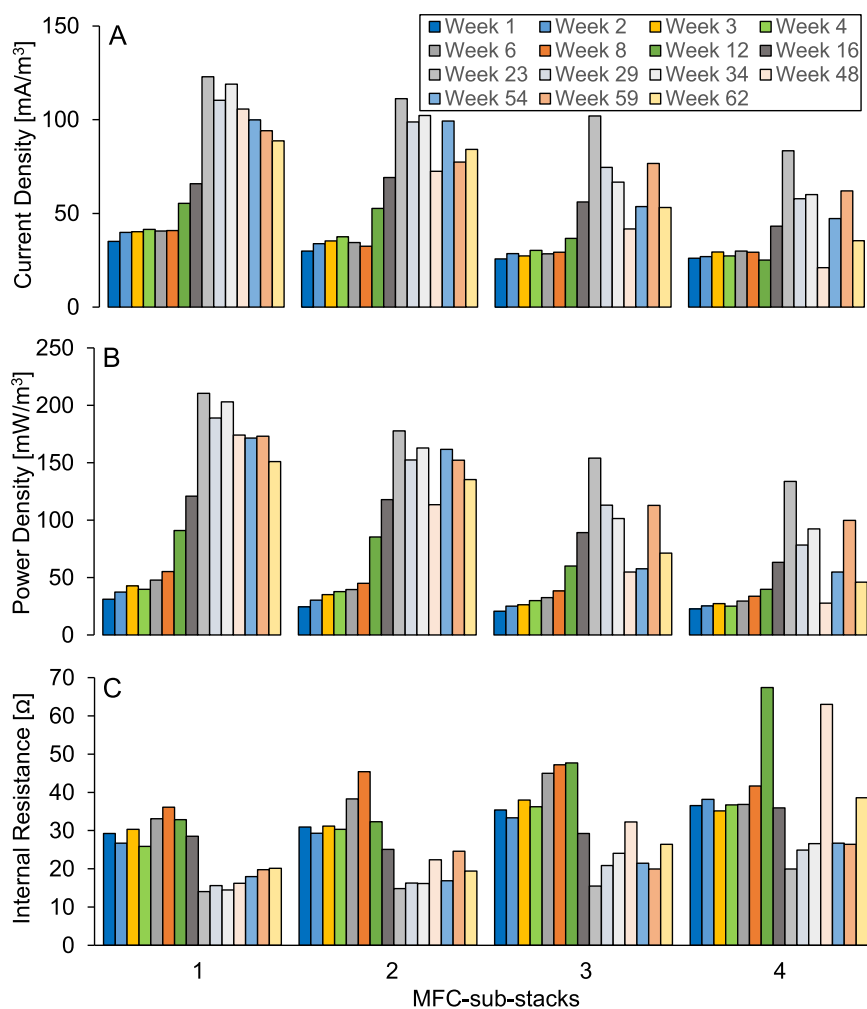


Fig. 2. Polarisation data, until week 12 acclimatisation period, then implementing four MPPT devices, one per MFC-sub-stack. Wastewater flow through the MFC-sub-stacks 1 to 4. A) Current at maximum power densities (P_{max}). B) P_{max} declined with water purification advancement. C) Internal resistances rose slightly with declining power generation.

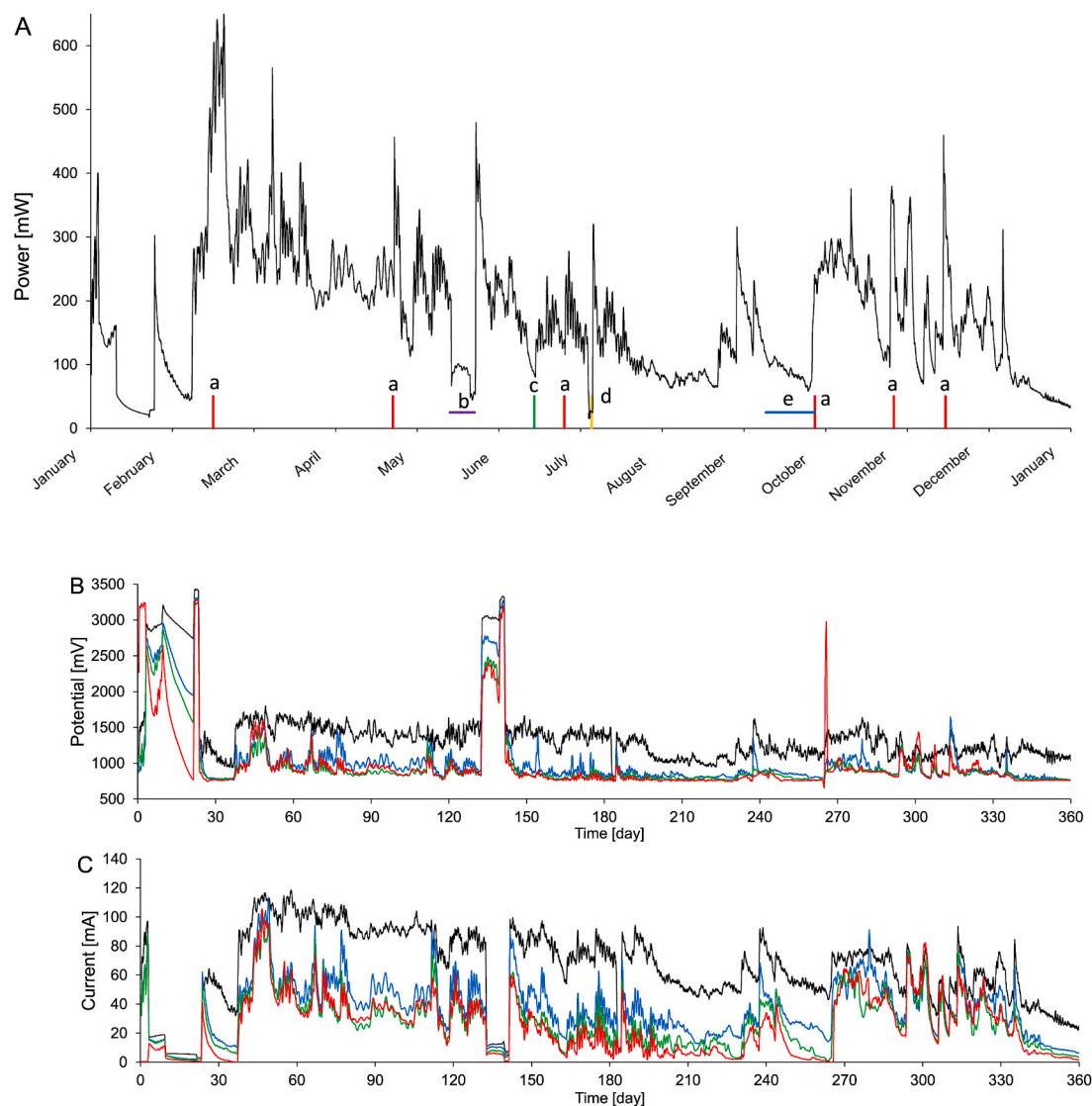


Fig. 3. A) Power generation using maximum power point tracking (MPPT) with the 1000-L MFC under continuous wastewater flow. Causes for power fluctuations: MFC units accumulated precipitated particles and were purged (a, red). Fix external resistance of 400 Ohm (b, violet). Reactor opening for microbiome sampling (c, green), air-O₂ supply interruption in cathodes (d, yellow). Grape harvest, unusual deposits and substrates impeded power generation (e, blue). B) Potentials per MFC-sub-stacks. C) Stack currents for all MFC-sub-stacks. Colours for MFC-sub-stack curves: 1 = black, 2 = blue, 3 = green, 4 = red. (For interpretation of the references to colour in this figure legend, the reader is referred to the Web version of this article.)

3.3. Power variations: intraday, weekly and others

Short term power variations originated for several reasons. Not all were explicable due to the sheer number of variations over time and the complexity of multiple parameter influences that changed by outside forces (Fig. 5). The COD in the wastewater varied in a sinusoidal manner during 24 hours and consequently changed the power. However, the COD was not measured in an automatized manner and the discussion was based on power data. During a typical week-day, COD and thus the power were highest around noon. In the following power declined and reached its lowest value during the night to rise again by up to ~80% (Fig. 5D). On weekends, these day/night power amplitudes were less pronounced as most businesses and public services connected to sewer system were closed down.

Another recurrent short term influence were heavy rainfalls, critically diluting the COD very much as the return to usual day/night oscillations lasted several days (Fig. 5D).

Several week long power declines were related to mounting deposits at the bottom of MFC units that began to cover anodes with time. This

led to fuel starvation on covered anode sections and less power was produced. Therefore, after 6, 8 and 10 months respective MFC units were purged from precipitates, later monthly purging was examined to maintain performance. Deposit removal restored power generation indicating that constant removal is required and MFC architecture needs to be adapted to this problem in order to remove sediments constantly.

There were many power changes not explicable and others perceived as expectable incidents. Several parameters potentially changed at the same moment and only a fully controlled system could reveal concluding information. For example, much changed wastewater composition or a chemical spills could affect power generation. In such cases the internal resistance of the MFC changes as the source power declines due to biocatalyst inhibition, denaturation or wrong fuel causing starvation effects. Under ordinary conditions, the MPPT adapted itself to changing fuel availability and internal resistances. The sensibility in the interplay of power generation and internal resistance variations was well seen when a fixed 400 Ohm external resistance replaced the MPPT routine (Fig. 3A, cause b). In the course of the yearlong experiment no toxic spill occurred. However, when the grape harvest

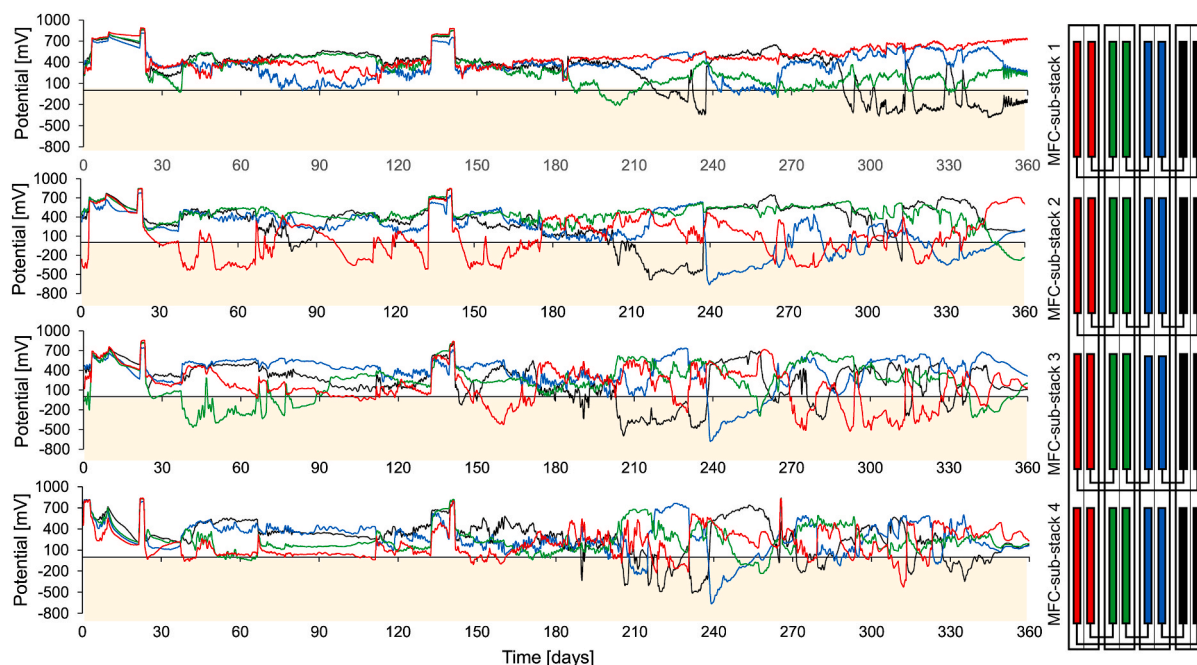


Fig. 4. MFC potentials per MFC-sub-stacks. Reversed voltages (<0.0 mV) became self-resolved with time. Right side: related MFC-sub-stacks to with electric connections in corresponding colours to the voltage data on the left side (wastewater flux form MFC-sub-stacks 1 to 4). (For interpretation of the references to colour in this figure legend, the reader is referred to the Web version of this article.)

started in fall, it was considered as a kind of chemical spill like moment. Grape harvest and pressing is launched in an officially well-defined time period. It is a recurrent problem for wastewater treatment plants in the region. The problem is usually attributed to an unusual sugar excess in wastewater and therefore such wastewater is separated and collected with the producers. However, there was nevertheless an unexpected problem for the MFC. The internal resistance of the MFC rose slowly and then exponentially while the COD increased just slowly to not very much higher level than usual. Less expected was a notable white turbidity of the wastewater. As a result, there was a constant power decline as sediments were formed faster than usual (Fig. 3A, cause e). This incident showed how important steady conditions were and that changes need an adaptation time as in today's aerated microbial WWTPs.

3.4. Voltage reversals

Voltage reversals were monitored for one year, which were self-healing. Rarely, there were periods without voltage reversal. The reversal type was mostly an imbalance among the MFC units in the stack. High currents, fuel starvation and corrosion like reversals, which were thought to occur were not clearly seen from obtained data. This was because the system was a flow thorough MFC with common electrolytes of constant composition. As the electrolytes in any specific location of the stretched MFC remained more or less the same for extended times the system was rather balanced. This analysis was confirmed by several observations. For example high currents were not affecting biofilms as seen in the first MFC-sub-stack (Fig. 4, top). The second often experienced fuel starvation phenomenon was seen in the 4th MFC-sub-stack (Fig. 4, bottom). Here low fuel supply (COD) was the normal state and therefore starvation induced reversals not likely. The third reversal type induced by corrosion of the electrode was neither seen. The observed voltage reversals were voltage imbalances inside serial MFC sub stacks (Fig. 4). They occurred probably due to different fluxes in the channels and biofilm growth with its own dynamics as seen from metagenomics data.

Reversals were usually compensated by a proportional counter rise of potential in one or more other MFCs in the same stack (Fig. 4, top =

MFC-sub-stack 1, see for example days 290–360). Voltage imbalances were in rare cases sharp voltage shifts among two units that affected the whole or more than one MFC-sub-stack (Fig. 4, see days 230–240). Voltage reversals, recoveries and shifts were not elucidated in the very moment as the system was run automatically for days. A number of interventions on the reactor (Fig. 3A, a-e) showed that imbalances could be triggered easily by the operator through mechanical incidents. These were mostly interrupted electrolyte fluxes causing starvation like reversals or otherwise said source power problem for a specific MFC unit or a number of them.

3.5. Seasonal influences on power generation

The 1000-L MFC was run for 1.5 years without interruption with wastewater and its changing characteristics over time. Seasonal influences on power generation were observed mostly due to varied rainfall frequencies and temperature alternations (Fig. 5C). Both of these parameters changed slowly, although rainfalls were sometimes heavy, regular rainfalls became more frequent reaching midsummer (Fig. 5A). Consequently, daily arriving wastewater volumes rose in the summer (Fig. 5A) and COD was proportionally more diluted. At some point, more wastewater was equally received in winter due to infrequent enhanced snow melting periods. Wastewater was diluted by these events as the sewer system was not designed to fully prevent rainwater intake.

The temperature changed by 1–2 °C per month and declined to 11.5 °C in February, before rising back to 21 °C in July (Fig. 5C). Temperature influenced the digestion kinetics of the COD in the anodic biofilms and more power was generated per COD (Fig. 5B). A 10 °C rise accounts in chemistry, in the given temperature range, a doubled substrate conversion. In fact, anodic COD conversions were eventually twice as fast depending which months were compared with each other. This rather qualitative observation needs to be seen by the fact that there was also a higher COD dilution in summer. This was in line with MPPT recordings, where the power curve (Fig. 3) declined in summer as less COD was contained per wastewater volume.

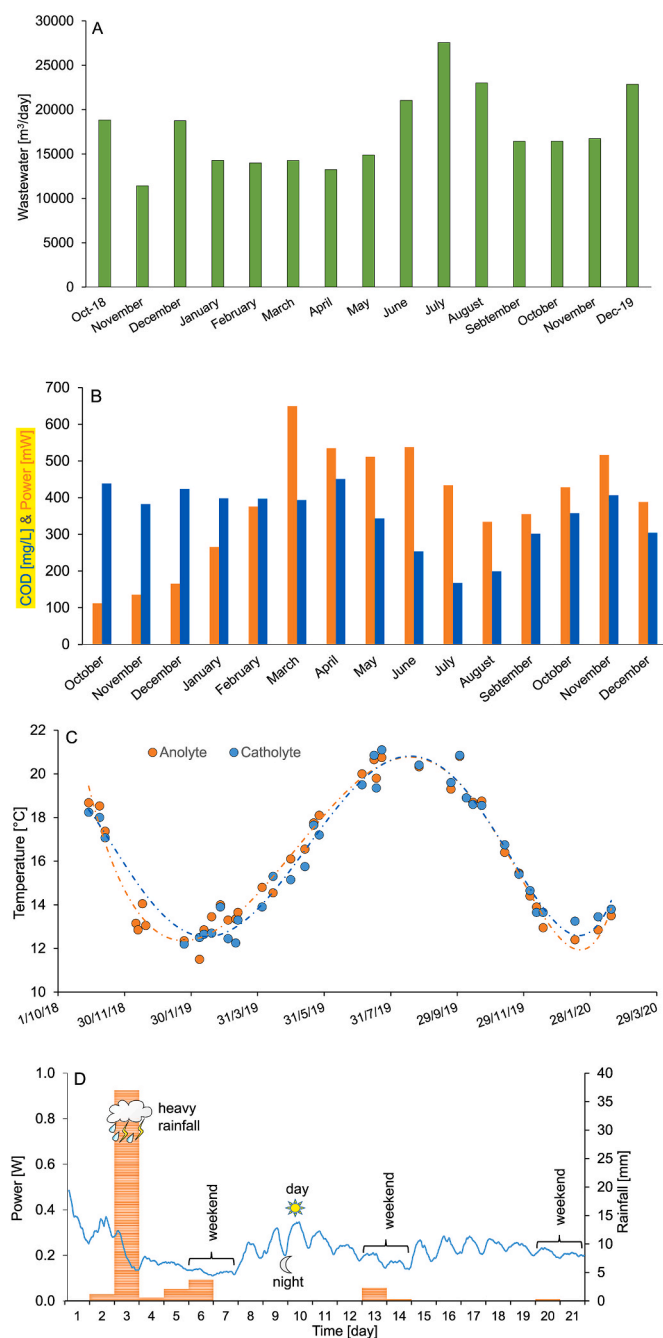


Fig. 5. 1000-L MFC and external influences. A) Rain and wastewater volume arriving in WWTP over time. It increased in summer, while COD per m³ wastewater declined (B). B) Maximum powers almost doubled in relation to COD concentrations with raising temperatures (e.g. April vs. July). C) Temperatures in 1000-L MFC, anode (orange) and cathode (blue). D) Three weeks power generation profile with daily changes and rainfalls. With the 3rd day power declined and remained flat as a result of heavy rainfall. (For interpretation of the references to colour in this figure legend, the reader is referred to the Web version of this article.)

3.6. Cathodic oxygen regulation

Oxygen consumption in the MFC cathode was reduced step by step to 12.8 kg O₂/d and was clearly lower than the 51.0 kg O₂/d used in open lagoon treatment. This was a clear improvement and confirmed the assumption that substantial power savings are possible with an aqueous cathode. As stated, the here performed value comparison concerned two very different system sizes and methods of operation; 17500 m³/d-

WWTP versus 0.5 m³/d with the 1000-L MFC-cathode.

Adjusted oxygen concentrations in MFC cathodes ensured highest possible power generation as at this point O₂ penetration through the CEM into the anode was minimized (Fig. 6). The double chambered MFC enabled anodic/cathodic oxygen regulation. The used VANADion membrane was not reported for MFC use. But an experimental comparison with the well suited Nafion N117 membrane showed that the VANADion membrane performed similarly. It was then chosen due to similar properties and its five times lower price.

3.7. Anolyte pH drop and its rise in catholyte

The pH of influent wastewater dropped from 7.2 to 6.7 through power generation. This drop was most pronounced in the first MFC-sub-stack (3 m long) and continued to a much lower degree in following MFC-sub-stack (Fig. 6C). In the following units the pH hardly changed anymore as much less electrogenic power was generated in the second half of the 1000-L MFC. The pH drop resulted from microbial organic matter oxidation by electrogenic microbes that liberated protons whose migration into the cathode was slow. The liberated protons were retained in biofilms and by the carbonate equilibrium in wastewater. Moreover, other cationic species close to the membranes easily replaced protons and migrated instead through the membrane. These replacing cations were Na⁺, K⁺, Ca²⁺, Mg²⁺, and ammonia. The opposite process occurred in the cathode, there the pH increased from 7.5 to 7.9 due to the same hindered proton migration. All in all, pH values remained upon initial change stable and microbial activity possible.

3.8. Power from organic matter: influence of maximum power point tracking

Water purification was mostly seen as COD conversion into power. However, a lot of COD conversion did not result in power for a number of reasons. To optimize this conversion into electricity maximum power point tracking (MPPT) was implemented. It was used to automatize constant P_{\max} approximations and the MFC worked by this function at best power generation levels. With this tool the internal resistance in the entire MFC tended to low values but still varied along with intraday COD variations. This automatized fine-tuned optimisation by the MPPT what was not possible to regulate manually. P_{\max} and internal resistances were nevertheless periodically determined manually by polarisation experiments. These internal resistances showed a somewhat increasing trend from the first to the fourth MFC-sub-stack (Fig. 2C). The reason was that electrogenic properties of the microbiomes declined toward later sections of the MFC. There, other microbial functionalities became important such as the degradation of more inert organic matter including micropollutants. Increasing mass transfer limitations contributed in addition to reduced power generation and internal resistance increased.

3.9. Particulate organic matter and power generation efficiencies and predictions

Best possible powers were estimated from inlet COD and removal measurements at the outlet of the reactor. This resulted in a rough assessment of the power efficiency which was found to be 5.8–12.1%. The higher value belonged to the best recorded in the field of scale up MFCs but both were probably underestimated (Table 3, entry 9). For a more accurate power assessment a mass balance would be needed but was not possible to establish. Nevertheless, the larger size offered deeper insights into MFC's redox reactions and other phenomenon.

All digestion related redox reactions are thought to contribute to anodic currents and would result in 100% Coulombic efficiency. In such a case the CE values are directly proportional to COD removal. A reason for limited COD to power conversions was partly organic matter precipitation in the MFC units. Although wastewater passed through a large

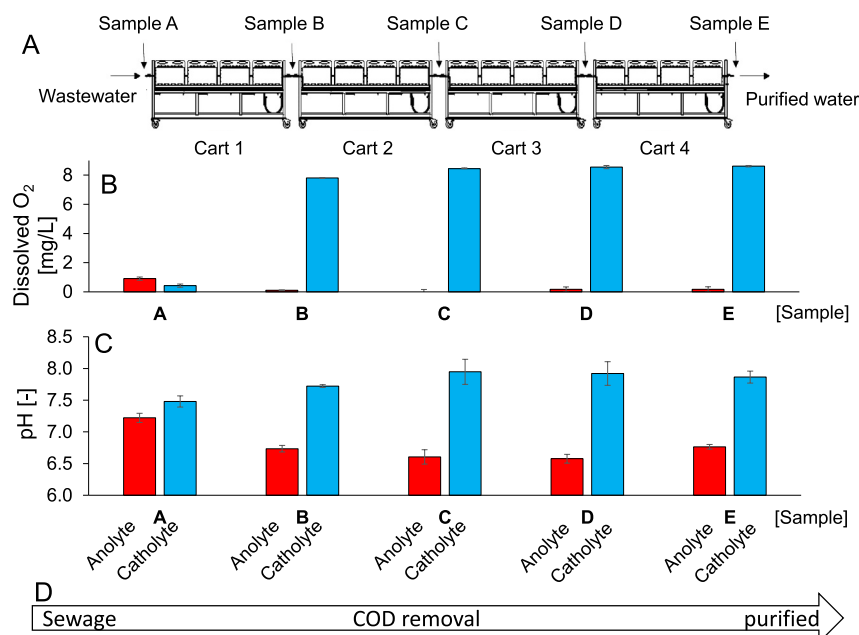


Fig. 6. Oxygen and pH in anodes and cathodes during power generation and wastewater purification within 12 m long common electrolyte channels. A) 1000-L MFC, arrows indicate sampling points. B) Oxygen concentrations in anodes (red) and cathodes (blue). C) pH in anodes (red) and cathodes (blue). D) Direction of wastewater flux with declining COD and increasing purity. (For interpretation of the references to colour in this figure legend, the reader is referred to the Web version of this article.)

decanter before entering the MFC it contained particles not available for anodic biofilms, what reduced power generation efficiencies. Sedimenting particles contained degradable matter and with time methane evolved when not removed, confirming that efficiency calculations were not exact. Accumulated precipitates were purged from concerned MFC units to re-establish power generation and purification.

3.10. Hydraulic retention time and power generation

To reach low COD values from anodic digestion wastewater flux needs to be adjusted to reach legal COD thresholds: < 45–60 mg/L and

>80–85% removal. Such adaptation optimized maximum powers (W/m^3) and Coulombic efficiencies (Fig. 7). A wastewater-MFC should be operated under constant wastewater flux. Coulombic efficiency versus power variability showed proportional changes with flux alternations. In one instance the anolyte flow rate was well reduced to 1.3 L/h resulting in a Coulombic efficiency of 14.9%. Conversely, accelerating the flow rate to 40 L/h the Coulombic efficiency dropped to 4.7%. Both Coulombic efficiencies were considered extreme values as in one case the process was too slow in view of the state of the art of WWT and in the other COD removal was clearly incomplete. As a compromise, the anolyte flow rate was fixed to 20 L/h for most of the time. This ensured at least 80% of COD removal and values up to 95% were possible. The CE-values corresponded to formerly recorded scale-up MFC data (volume > 10 L) reaching 1–20% [30–33] and in one case 53% CE [34]. However, the Coulombic efficiency is hardly a telling parameter to predict power generation of a larger MFC reactor. Coulombic efficiency can be optimized under batch conditions by bubbling air-O₂ through the cathode for extended times. Batch conditions and low wastewater fluxes inflate MFC size and turns the system non-economic. The hydraulic retention time needs, from current perspective, to be constantly monitored and controlled to enhance performance.

3.11. Bioanodic redox reactions in competition with air-oxygen and metal cations

In the quest for enhanced energy efficiencies, a number of MFC processes need closer examination. Unwanted redox reactions could play a central role in both half cells, even though the cathode was less complex to assess than the anode. The most feared power loss mechanism was routed in the competing oxidation of organic matter by leaking air-oxygen into the anode. This unwanted biocatalysis was enabled by oxygen respiring microbes incorporated in biofilms due to certain level of air-oxygen in the anode. Therefore, oxygen was excluded as completely as possible by reducing cathodic air-oxygen supply to a strict minimum.

However, oxygen was already contained in influx wastewater with 0.9 mg/L due to the air exposed sewer system, including sand and

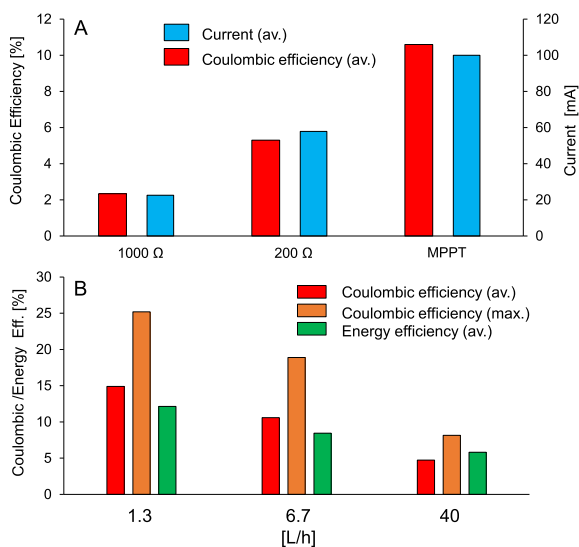


Fig. 7. Coulombic and energy efficiencies with the 1000-L MFC. A) Lowering external resistances increased currents and Coulombic efficiencies. B) Higher wastewater flux reduced Coulomb efficiencies and enhanced energy efficiencies proportionally although both declined.

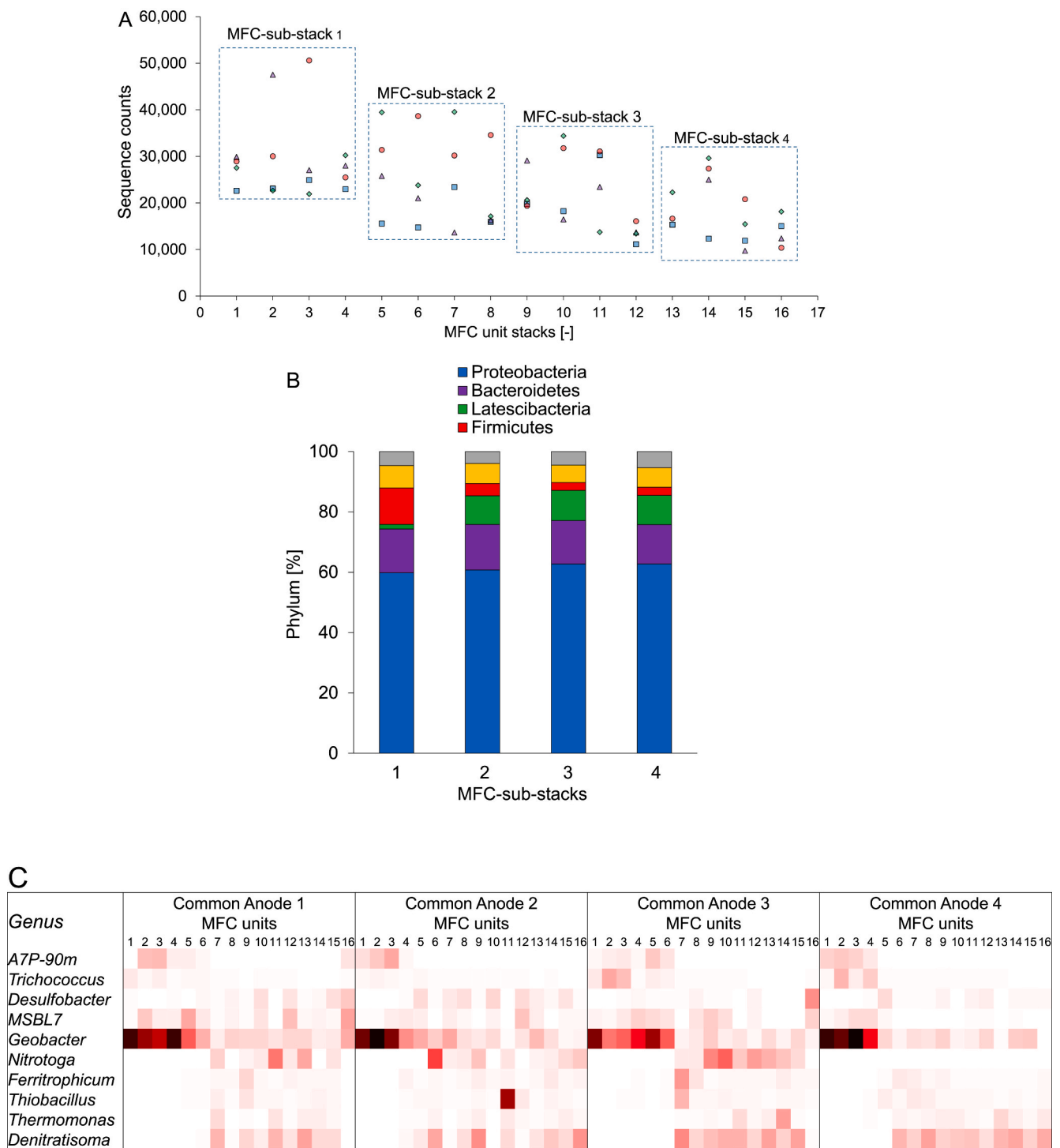


Fig. 8. A) OTU based amplicons (sequence) read plot with population changes at 16 sampling points in the 12 m long common anodes 1–4 with a wastewater flux of 20 L/h, (from left to right). The distance from one microbiome sample to the next was ~80 cm. Marker code for common anode channels: a, ■, b, ▲, c, ◆, d, ●. B) Phylum in the four MFC-sub-stacks. C) Heatmap of 10 most dominant genus in the four common anode channels. The threshold for genus inclusion was ≥5% occurrence in at least one of 64 MFC microbiome samples. Colour code: 0% (white) to 60% (black). (For interpretation of the references to colour in this figure legend, the reader is referred to the Web version of this article.)

Table 1

In-out concentrations of nitrogen compounds with the 1000-L MFC. Process conditions: anolyte wastewater flow rate = 20 L/h and catholyte = 2 L/h. Cathode values were normalized with anode data for direct comparison.

N-solutes	Anolyte _{in}	Anolyte _{out}	Catholyte _{in}	Catholyte _{out}	Legal threshold
NH ₄ ⁺ [mg/L (mmol/L)]	28.7 (1.59)	13.9 (0.77)	0.003	0.005	2.0
NO ₂ ⁻ [mg/L (μmol/L)]	0.03 (0.6)	0.02 (0.4)	0.001	0.001	0.3
NO ₃ ⁻ [mg/L (μmol/L)]	0.09 (1.0)	0.07 (1.0)	0.081 (1.0)	2.90 (4.6)	N/A

Table 2

Anodic DNA extracts with the 1000-L MFC. Toward the outlet port of the reactor (MFC sub-stack 4) almost twice as much DNA (see bottom line) than in the first section (MFC-sub-stack 1). Each anode channel (a-d) was 12 m long, each extract represents a 3 m long section in one of the anode channels (a-d).

Anode channels	DNA extracts per MFC-sub-stacks			
	1	2	3	4
			[μg/L]	
a	4.45	7.18	7.30	11.41
b	3.90	6.70	10.2	8.94
c	5.18	7.03	5.18	5.92
d	5.78	4.37	3.70	7.43
Average	4.83	6.32	6.60	8.42

particle decanters. The mechanical removal of unwanted oxygen in influents was considered more costly than its removal by in-process microbial reduction. This oxygen was removed in the first MFC-sub-stack (Fig. 6B). The second reason for oxygen in the anolyte was its migration from the cathode through the CEM as expected. The oxygen content in the cathode was regulated exploiting the advantage of the aqueous cathode (Fig. 6B). But still, O₂ migration into the cathode was observed in MFC-sub-stacks 3 and 4 where O₂ concentration remained constant at 0.17 mg/L. To achieve lower oxygen contents would require automated control and adjustment.

Another sizable electron sink were metal cations, reducible under anaerobic conditions by electrogenic microbes [26]. This concerned in particular Fe³⁺, which was added artificially as FeCl₃ before wastewater entered the MFC in order to remove phosphate. FeCl₃ reacted with phosphate and precipitated as strengite (FePO₄). Depending on the hydraulic rate Fe³⁺ was reduced to Fe²⁺ resulting in even less soluble vivianite (Fe₃(PO₄)₂) [35]. The importance of this electron sink was estimated to correspond to one equivalent of electrons per equivalent of phosphate if not overdosed. Other reducible metal cations were present too but in trace amounts and their eventual reduction was considered insignificant to impact power generation. All in all, the energy efficiency of the 1000-L MFC could be higher by enhanced air-oxygen control.

Table 3

Comparison of the 1000-L MFC with other scale-up MFCs. ^aCalculated values from reported data.

Entry	MFC [L]	Wastewater Type	Realized Energy Density [kWh/m ³] [kWh/kg COD]	COD Removal [%]	Coulombic Efficiency [%]	Energy Efficiency [%]	[References] (Year)
1	10	Brewery	0.200 ^a	0.109 ^a	87.1	6.3–7.6	[32](2012)
2	20	Brewery	0.030–0.310	0.033–0.359	47.6–94.5	5.5–53.6	[33](2017)
3	90	Brewery	0.056–0.097	0.033	82.7–86.5	8.0–19.1	[31](2015)
4	20	Municipal	0.004	0.011	66–80	0.30	[50](2011)
5	45	Municipal	0.007–0.025	0.360	13.5–67.0	10.1–24.8	[51](2016)
6	250	Municipal	0.054	0.206	79	3–7	[30](2014)
7	1000	Municipal	0.015 ^a	0.242 ^a	70–80	41–75	[52](2018)
8	72	Synthetic	0.071–0.131 ^a	0.194–0.473 ^a	78–97	1–14	[33](2016)
9	1000	Municipal	0.015–0.060	0.224–0.469	34.4–95.4	4.7–14.9	5.8–12.1 This work

3.12. Nitrification and denitrification

Ammonia oxidation and subsequent nitrate denitrification started according to metagenomics mapping in the 1000-L MFC once the COD was well reduced (Fig. 8). Ammonia is an ecotoxic compound and has to be removed below a threshold of 2.0 mg/L to fulfil legal requirement. Its removal was partly achieved with 48.4% at a 20 L/h wastewater flux. It was oxidized into nitrite and nitrates, as registered data confirmed (Table 1). The intermediate nitrite was transformed into nitrate and then reduced into nitrogen. Unexpectedly, nitrate accumulated in the cathode, what was a result of ammonia migration through the CEM. Cathodic ammonia was largely oxidized into nitrate. This process needs more attention as unexpectedly denitrifying microbes were found on cathodes.

3.13. Anodic microbiome structure and metabolism

Metagenomic sequencing of anodic biofilms was performed in the 9th month of uninterrupted reactor use. The anodic microbiome composition of all 64 MFC units of the 1000-L MFC was examined by the 16S rRNA V4–V5 method. This resulted in an anodic microbiome map of the entire 1000-L MFC. It provided novel insights into the microbiome structure with the stretched out MFC system (Fig. 1) and resulted in an unprecedented view into principal metabolic pathways in bioelectricity supported wastewater digestion.

DNA extracts represented a tiny fraction of all anodic biofilms but nevertheless reflected the reality as they were sampled in a pseudo quantitative manner. The microbiomes were cut out from RVC surfaces as small disks (2 × 0.8_d cm as a fraction of a total projected anode surface of 273 cm²). Unexpectedly, more DNA was extracted toward the end of the 12 m long 1000-L MFC reactor than with the beginning where metabolic activity was obviously much more intense (Table 2). This DNA-mass asymmetry was related to the fact that the microbiome property changed with purification progress. But why the biofilms became thicker and not thinner? In the first three to five meters of the anode channels the electrogenic genera *Geobacter* [36] was present in up to 60% (Fig. 8A). The hypothesis was, that they respire with the surface and the respiration for electrogens in some distance to the electrode made electron transfer impossible. The opposite was true for aerobic microbes in the later part of the reactor as they best respired with anolyte that contained traces of oxygen and they grew thicker for this reason.

One of a well present but not dominant genus was *A7P-90 m* [37]. It coexisted with *Geobacter* and is a proteolytic genus liberating ammonia and other compounds. From the heatmap (Fig. 8C) it can be seen, in a quite striking fashion, that other microbes gained their presence when *Geobacter* lost its predominant role due to substantial COD removal. In these later sections, in particular nitrifying and denitrifying bacteria were detected in good quantities. These were the genera *Candidatus nitroga* [38], *Denitratisoma* [39] as well as *Thermomonas* [40] converting ammonia into nitrite and nitrate. The denitrifying function was equally visible and nitrate was well removed from wastewater (Table 1).

Sulphur reducers were equally detected in sizable amounts, in particular *Desulfobacter* [41], *MSBL7* [42] and *Thiobacillus* [43]. *Thiobacillus* was of additional interest as an iron leach microbe. Its presence was related to the applied phosphate removal method used in this work. Phosphate was chemically removed by FeCl_3 addition before wastewater entered the MFC. Fe^{3+} complexed and precipitated phosphate as FePO_4 which is in anaerobic conditions easily reduced to $\text{Fe}_3(\text{PO}_4)_2$. Once Fe^{2+} remained, it was eventually oxidized by *Ferritrophicum* [44]. This indicated that biofilms were not phosphate limited but still enabled standard phosphate recovery to fulfil legal standards.

The operational taxonomic units (OTUs), respectively the related amplicon reads, showed declining species populations with purification progress (Fig. 8A). This showed, that the biofilm was thicker in this section than the DNA extraction indicated and according OTUs counting species diversity dropped from average 385 to 364 per anode.

In conclusion, metagenomic microbiome mapping of all bioanodes enabled to distinguish two obvious sections of digestive activities like not seen before. The application of a threshold of 5% on genus data resulted in a selection on 10 most important genera needed for bioelectric municipal WWT.

3.14. The cathode's microbiome

Biofilms were unexpectedly found on cathodes during microbiome sampling from anodes. The air-oxygen cathodes were not designed to become biocathodes. They became exposed to microbes from the groundwater used as catholyte. Sizable quantities of DNA material was extracted from four samples on the first four cathodes adjacent to the inlets of the 1000-L MFC. And four samples from the last four cathodes, at the outlet ports. The DNA extracts showed in contrast to the anodes that biofilms were thicker at the inlets than at the other end of the reactor. This thickness difference was a result of a biofilm growth in well oxygenated water and seemed rather a nuisance than of practical use.

However this was not the whole truth. A smaller number of microbial genera were detected in comparison to anode electrodes (at least 5% per genera in one of 8 samples). The cathodic biofilm seemed to be adapted to denitrifying ammonia. Ammonia migrated into the cathode and was oxidized into nitrate as analytical data proved (Table 1). This observation was confirmed by the presence of microbes, mostly denitrifiers such as *Nitrospira* [45], the most abundant. Another denitrifier genus with minor relative abundance was *Thiothrix* [46]. The similar function executed the genus *Nitrosomonas* [47], an ammonia oxidizer. Other genera were less WWT process adapted such as *Methylomagnus* [48] which is a methane and methanol oxidizer. The same was true for the genus *OLB12* [49], whose MFC related function was equally not assigned.

3.15. Perspective on further scale up of microbial fuel cells

The 1000-L MFC was run for over a year with low maintenance needs. The question was in fact what was achieved in view of an eventual implementation at the examined or a larger scale? This already quite large MFC reactor was in reality still small in contrast to wastewater treatment capacities required for municipal WWT. Based on this, the 1000-L MFC could be useful in remote places. There, the higher construction cost and space requirements are less difficult to justify than to build larger units for municipalities. An important cost cutting factor will be ultimately power generation and electricity savings. Because both reduce operation cost and could change the state of the art in WWT. The average power generated from wastewater was only 0.015 kWh/m^3 . A value far from the energy potential of most wastewaters. Conversely, power savings appear easier to accomplish but this is not yet proven in detail.

An electricity production and saving calculation based on realized 0.015 kWh/m^3 and for the 45000 people equivalents of the WWTP Châteauneuf showed that 95800 kWh/y of electricity could be

produced. With $17500 \text{ m}^3/\text{d}$ of wastewater, the electricity consumption of 18 households (5200 kWh/y) could be covered. Additional saving could be achieved by adjusting air-oxygen in the MFC, as an assumption 75%, the power of 110 additional household equivalents could be saved.

As in the state to the art WWTP, there remained two legally limited pollutants in purified wastewaters. These were ammonia and organic micropollutants. In contrast to today's WWTP, there are additional noteworthy features of MFCs. The MFC-WWTP nullifies volatile pollutant stripping into the air and enables CO_2 recycling from exhaust gas.

4. Conclusions

The 1000-L MFC produced electricity, purified wastewater and saved power. Power generation was assisted by maximum power point tracking and 0.015 kWh/m^3 of electricity were obtained on a regular basis with peak performance of up to 0.060 kWh/m^3 . The energy efficiency was 5.8%–12.1%, what was the highest value so far for scale-up MFCs fed with municipal wastewater. Voltage reversals were self-healing with time in all instances, in some MFC sections they were more persistent than with others. The microbiome's structure and metabolism changed with purification progress in a somewhat bi-sequential manner not seen before. Initially, electrogenic *Geobacter* dominated power generation and then nitrification, denitrification and desulfurization set in too. Beside this, fermentative microbes were equally present. Overall, 10 dominant genera were identified by microbiome mapping. They were involved in bioelectric power generation and wastewater purification. Higher OTUs/sequence reads were found in the beginning of the MFC process and then the microbial presence declined with purification progress. While anodic DNA extracts indicated thicker biofilms with purification progress.

The COD removal reached legal requirements with up to 95%. Ammonia was removed by 48% and organic micropollutants were reduced by 65%. All in all, the scale-up 1000-L MFC generated power, reduced electricity consumption, cleaned wastewater and avoided volatile pollutant stripping into the air and is a future source for concentrated CO_2 .

CRedit authorship contribution statement

Maxime Blatter: Investigation, Formal analysis, Writing - original draft. **Louis Delabays:** Software, programming, Investigation. **Clément Furrer:** Investigation. **Gérald Huguenin:** Conceptualization, Supervision. **Christian Pierre Cachelin:** Investigation. **Fabian Fischer:** Conceptualization, Funding acquisition, Supervision, Project administration, Writing - review & editing.

Declaration of competing interest

The authors declare that they have no known competing financial interests or personal relationships that could have appeared to influence the work reported in this paper.

Acknowledgements

This work was supported by the Swiss Federal Office of Energy (SI/501573-01), "The Ark" foundation, the HESSO Valais and the WWTP Châteauneuf. We thank the construction team of the polymechanic shop of HES-SO Valais and the wastewater treatment plant of the City of Sion and its crew for multiple help and the accommodation of the 1000-L MFC.

References

- [1] S. Longo, B. d'Antoni, M. Bongards, A. Chaparro, A. Cronrath, F. Fatone, J. Lema, M. Mauricio-Iglesias, A. Soares, A. Hospido, Monitoring and diagnosis of energy

- consumption in wastewater treatment plants. A state of the art and proposals for improvement, *Appl. Energy* 179 (2016) 1251–1268, <https://doi.org/10.1016/j.apenergy.2016.07.043>.
- [2] J. Elias-Maxil, J. van der Hoek, J. Hofman, L. Rietveld, Energy in the urban water cycle: actions to reduce the total expenditure of fossil fuels with emphasis on heat reclamation from urban water, *Renew. Sustain. Energy Rev.* 30 (2014) 808–820, <https://doi.org/10.1016/j.rser.2013.10.007>.
- [3] G. Venkatesh, H. Brattebo, Energy consumption, costs and environmental impacts for urban water cycle services: case study of Oslo (Norway), *Energy* 36 (2011) 792–800, <https://doi.org/10.1016/j.energy.2010.12.040>.
- [4] P. Gikas, Towards energy positive wastewater treatment plants, *J. Environ. Manag.* 203 (2017) 621–629, <https://doi.org/10.1016/j.jenvman.2016.05.061>.
- [5] P.L. McCarty, J. Bae, J. Kim, Domestic wastewater treatment as a net energy producer—can this be achieved? *Environ. Sci. Technol.* 45 (2011) 7100–7106, <https://doi.org/10.1021/es2014264>.
- [6] H. Liu, R. Ramnarayanan, B. Logan, Production of electricity during wastewater treatment using a single chamber microbial fuel cell, *Environ. Sci. Technol.* 38 (2004) 2281–2285, <https://doi.org/10.1021/es034923g>.
- [7] M. Wakeel, B. Chen, T. Hayat, A. Alsaedi, B. Ahmad, Energy consumption for water use cycles in different countries: a review, *Appl. Energy* 178 (2016) 868–885, <https://doi.org/10.1016/j.apenergy.2016.06.114>.
- [8] F. Zhang, Z. Ge, J. Grimaud, J. Hurst, Z. He, Long-term performance of liter-scale microbial fuel cells treating primary effluent installed in a municipal wastewater treatment facility, *Environ. Sci. Technol.* 47 (2013) 4941–4948, <https://doi.org/10.1021/es400631r>.
- [9] F. Zhang, Z. Ge, J. Grimaud, J. Hurst, Z. He, In situ investigation of tubular microbial fuel cells deployed in an aeration tank at a municipal wastewater treatment plant, *Bioresour. Technol.* 136 (2013) 316–321, <https://doi.org/10.1016/j.biortech.2013.02.107>.
- [10] A. Cucu, A. Tiliakos, I. Tanase, C. Serban, I. Stamatina, A. Ciocanea, C. Nichita, R. Damian, Microbial fuel cell for nitrate reduction, *Eenviro-Yrc* 2015 - Bucharest 85 (2016) 156–161, <https://doi.org/10.1016/j.egypro.2015.12.286>.
- [11] M. Arredondo, P. Kuntke, A. Jeremiase, T. Sleutels, C. Buisman, A. ter Heijne, Bioelectrochemical systems for nitrogen removal and recovery from wastewater, *Environ. Sci. Water Res. Technol.* 1 (2015) 22–33, <https://doi.org/10.1039/C4EW00066H>.
- [12] M. Blatter, M. Sugnaux, C. Comninellis, K. Neelson, F. Fischer, Modeling of sustainable base production by microbial electrolysis cell, *ChemSusChem* 9 (2016) 1570–1574, <https://doi.org/10.1002/cssc.201600459>.
- [13] G. Palanisamy, H. Jung, T. Sadhasivam, M.D. Kurkuri, S.C. Kim, S.H. Roh, A comprehensive review on microbial fuel cell technologies: processes, utilization, and advanced developments in electrodes and membranes, *J. Clean. Prod.* 221 (2019) 598–621, <https://doi.org/10.1016/j.jclepro.2019.02.172>.
- [14] H. Hiegemann, T. Littfinski, S. Krimmler, M. Lübken, D. Klein, K.G. Schmelz, O. Kristoffer, P. Deepak, M. Wichern, Performance and inorganic fouling of a submerged 255 L prototype microbial fuel cell module during continuous long-term operation with real municipal wastewater under practical conditions, *Bioresour. Technol.* 294 (2019) 122227.
- [15] M. Aghababae, M. Farhadian, A. Jehanipour, D. Biria, Effective factors on the performance of microbial fuel cells in wastewater treatment—a review, *Environ. Technol. Rev.* 4 (2015) 71–89, <https://doi.org/10.1080/09593330.2015.1077896>.
- [16] S.-E. Oh, B.E. Logan, Voltage reversal during microbial fuel cell stack operation, *J. Power Sources* 167 (2007) 11–17, <https://doi.org/10.1016/j.jpowsour.2007.02.016>.
- [17] J. An, J. Sim, H.-S. Lee, Control of voltage reversal in serially stacked microbial fuel cells through manipulating current: significance of critical current density, *J. Power Sources* 283 (2015) 19–23, <https://doi.org/10.1016/j.jpowsour.2015.02.076>.
- [18] M. Sugnaux, C. Savy, C.P. Cachelin, G. Huguenin, F. Fischer, Simulation and resolution of voltage reversal in microbial fuel cell stack, *Bioresour. Technol.* 238 (2017) 519–527, <https://doi.org/10.1016/j.biortech.2017.04.072>.
- [19] J. Li, H. Li, Q. Fu, Q. Liao, X. Zhu, H. Kobayashi, D. Ye, Voltage reversal causes bioanode corrosion in microbial fuel cell stacks, *Int. J. Hydrogen Energy* 42 (2017) 27649–27656, <https://doi.org/10.1016/j.ijhydene.2017.05.221>.
- [20] F. Khaled, O. Ondel, B. Allard, F. Buret, Voltage balancing strategies for serial connection of microbial fuel cells, *Eur. Phys. J. Appl. Phys.* 71 (2015) 10904, <https://doi.org/10.1051/epjap/2015150044>.
- [21] F. Fischer, M. Sugnaux, M.C. Savy, G. Huguenin, Microbial fuel cell stack power to lithium battery stack: pilot concept for scale up, *Appl. Energy* 230 (2018) 1633–1644, <https://doi.org/10.1016/j.apenergy.2018.09.030>.
- [22] B. Erable, L. Etcheverry, A. Bergel, From microbial fuel cell (MFC) to microbial electrochemical snorkel (MES): maximizing chemical oxygen demand (COD) removal from wastewater, *Biofouling* 27 (2011) 319–326, <https://doi.org/10.1080/08927014.2011.564615>.
- [23] M. Blatter, C. Furrer, C.P. Cachelin, F. Fischer, Phosphorus, chemical base and other renewables from wastewater with three 168-L microbial electrolysis cells and other unit operations, *Chem. Eng. J.* 390 (2020) 124502, <https://doi.org/10.1016/j.cej.2020.124502>.
- [24] Y. Yang, L. Yan, J. Song, M. Xu, Optimizing the electrode surface area of sediment microbial fuel cells, *RSC Adv.* 8 (2018) 25319–25324, <https://doi.org/10.1039/C8RA05069D>.
- [25] B. Logan, B. Hamelers, R. Rozendal, U. Schröder, J. Keller, S. Freguia, P. Aelterman, W. Verstraete, K. Rabaey, Microbial fuel cells: methodology and technology, *Environ. Sci. Technol.* 40 (2006) 5181–5192, <https://doi.org/10.1021/es0605016>.
- [26] D. Ucar, Y. Zhang, I. Angelidaki, An overview of electron acceptors in microbial fuel cells, *Front. Microbiol.* 8 (2017) 643, <https://doi.org/10.3389/fmicb.2017.00643>.
- [27] Z. He, Development of microbial fuel cells needs to go beyond "power density, *ACS Energy Lett.* 2 (2017) 700–702, <https://doi.org/10.1021/acscenergylett.7b00041>.
- [28] Z. Ge, J. Li, L. Xiao, Y. Tong, Z. He, Recovery of electrical energy in microbial fuel cells: brief review, *Environ. Sci. Technol. Lett.* 1 (2013) 137–141, <https://doi.org/10.1021/ez4000324>.
- [29] Y. Scherson, C. Criddle, Recovery of freshwater from wastewater: upgrading process configurations to maximize energy recovery and minimize residuals, *Environ. Sci. Technol.* 48 (2014) 8420–8432, <https://doi.org/10.1021/es501701s>.
- [30] Y. Feng, W. He, J. Liu, X. Wang, Y. Qu, N. Ren, A horizontal plug flow and stackable pilot microbial fuel cell for municipal wastewater treatment, *Bioresour. Technol.* 156 (2014) 132–138, <https://doi.org/10.1016/j.biortech.2013.12.104>.
- [31] Y. Dong, Y. Qu, W. He, Y. Du, J. Liu, X. Han, Y. Feng, A 90-liter stackable baffled microbial fuel cell for brewery wastewater treatment based on energy self-sufficient mode, *Bioresour. Technol.* 195 (2015) 66–72, <https://doi.org/10.1016/j.biortech.2015.06.026>.
- [32] L. Zhuang, Y. Yuan, Y. Wang, S. Zhou, Long-term evaluation of a 10-liter serpentine-type microbial fuel cell stack treating brewery wastewater, *Bioresour. Technol.* 123 (2012) 406–412, <https://doi.org/10.1016/j.biortech.2012.07.038>.
- [33] S. Wu, H. Li, X. Zhou, P. Liang, X. Zhang, Y. Jiang, X. Huang, A novel pilot-scale stacked microbial fuel cell for efficient electricity generation and wastewater treatment, *Water Res.* 98 (2016) 396–403, <https://doi.org/10.1016/j.watres.2016.04.043>.
- [34] M. Lu, S. Chen, S. Babanova, S. Phadke, M. Salvacion, A. Mirhosseini, S. Chan, K. Carpenter, R. Cortese, O. Bretschger, Long-term performance of a 20-L continuous flow microbial fuel cell for treatment of brewery wastewater, *J. Power Sources* 356 (2017) 274–287, <https://doi.org/10.1016/j.jpowsour.2017.03.132>.
- [35] P. Wilfert, A.I. Dugulan, K. Goubitz, L. Korving, G.J. Witkamp, M.C.M. Van Loosdrecht, Vivianite as the main phosphate mineral in digested sewage sludge and its role for phosphate recovery, *Water Res.* 144 (2018) 312–321, <https://doi.org/10.1016/j.watres.2018.07.020>.
- [36] S.I. Ishii, K. Watanabe, S. Yabuki, B.E. Logan, Y. Sekiguchi, Comparison of electrode reduction activities of *Geobacter sulfurreducens* and an enriched consortium in an air-cathode microbial fuel cell, *Appl. Environ. Microbiol.* 74 (2008) 7348–7355, <https://doi.org/10.1128/AEM.01639-08>.
- [37] E.V. Pikuta, Z. Lyu, R.B. Hoover, Y. Liu, N.B. Patel, H.J. Busse, P.A. Lawson, *Williamwhitmania taraxaci* gen. nov., sp. nov., a proteolytic anaerobe with a novel type of cytology from Lake Untersee in Antarctica, description of *Williamwhitmaniaceae* fam. nov., and emendation of the order *Bacteroidales* Krieg 2012, *Int. J. Syst. Evol. Microbiol.* 67 (2017) 4132–4145, <https://doi.org/10.1099/ijsem.0.002266>.
- [38] K. Kitzinger, H. Koch, S. Lückner, C.J. Sedlacek, C. Herbold, J. Schwarz, A. Daebeler, A.J. Mueller, M. Lukumbuzya, S. Romano, N. Leisch, S.M. Karst, R. Kirkegaard, M. Albertsen, P.H. Nielsen, M. Wagner, H. Daims, Characterization of the first “*Candidatus Nitrotoga*” isolate reveals metabolic versatility and separate evolution of widespread nitrite-oxidizing bacteria, *mBio* 9 (2018), <https://doi.org/10.1128/mBio.01186-18> e01186-18.
- [39] M. Fahrbach, J. Kuever, R. Meinke, P. Kämpfer, J. Hollender, *Denitratisoma oestradiolum* gen. nov., sp. nov., a 17 β -oestradiol-degrading, denitrifying betaproteobacterium, *Int. J. Syst. Evol. Microbiol.* 56 (2006) 1547–1552, <https://doi.org/10.1099/ijse.0.63672-0>.
- [40] J.H. Ju, J.S. Kim, D.H. Lee, J.H. Jeon, S.Y. Heo, J.W. Seo, C.H. Kim, D.S. Park, B. R. Oh, *Thermomonas aquatica* sp. nov., isolated from an industrial wastewater treatment plant, *Int. J. Syst. Evol. Microbiol.* 69 (2019) 3399–3404, <https://doi.org/10.1099/ijsem.0.003630>.
- [41] F. Widdel, New types of acetate-oxidizing, sulfate-reducing *Desulfobacter* species, *D. hydrogenophilus* sp. nov., *D. latus* sp. nov., and *D. curvatus* sp. nov. *Arch. Microbiol.* 148 (1987) 286–291, <https://doi.org/10.1007/BF00456706>.
- [42] E. Deja-Sikora, M. Gołębiewski, A. Kalwasińska, A. Krawiec, P. Kosobucki, M. Walczak, *Comamonadaceae* OTU as a remnant of an ancient microbial community in sulfidic waters, *Microb. Ecol.* 78 (2019) 85–101, <https://doi.org/10.1007/s00248-018-1270-5>.
- [43] L.G. Leduc, G.D. Ferroni, The chemolithotrophic bacterium *Thiobacillus ferrooxidans*, *FEMS Microbiol. Rev.* 14 (1994) 103–119, <https://doi.org/10.1111/j.1574-6976.1994.tb00082.x>.
- [44] J.V. Weiss, J. A. Rentz, T. Plaia, S.C. Neubauer, M. Merrill-Floyd, T. Lilburn, C. Bradburne, J.P. Megonigal, D. Emerson, Characterization of neutrophilic Fe (II)-oxidizing bacteria isolated from the rhizosphere of wetland plants and description of *Ferritrophicum radicolica* gen. nov. sp. nov., and *Sideroxydans paludicola* sp. nov. *Geomicrobiol. J.* 24 (2007) 559–570, <https://doi.org/10.1080/01490450701670152>.
- [45] M.J. Mehrani, D. Sobotka, P. Kowal, S. Ciesielski, J. Makinia, The occurrence and role of *Nitrospira* in nitrogen removal systems, *Biores. Technol.* 303 (2020) 122936, <https://doi.org/10.1016/j.biortech.2020.122936>.
- [46] I.V. Trubitsyn, E.V. Belousova, M.N. Tutukina, A.Y. Merkel, G.A. Dubinina, M. Y. Grabovich, Expansion of ability of denitrification within the filamentous colorless sulfur bacteria of the genus *Thiothrix*, *FEMS Microbiol. Lett.* 358 (2014) 72–80, <https://doi.org/10.1111/1574-6968.12548>.
- [47] P. Chain, J. Lamerdin, F. Larimer, W. Regala, Y. Lao, M. Land, H. Loren, A. Hooper, M. Klotz, J. Norton, L. Sayavedra-Soto, D. Arciero, H. Norman, M. Whittaker, D. Arp, Complete genome sequence of the ammonia-oxidizing bacterium and obligate chemolithoautotroph *Nitrosomonas europaea*, *J. Bacteriol.* 185 (2003) 2759–2773, <https://doi.org/10.1128/JB.185.9.2759-2773.2003>.

- [48] A. Khalifa, C.G. Lee, T. Ogiso, C. Ueno, D. Dianou, T. Demachi, A. Katayama, S. Asakawa, *Methylomagnum ishizawai* gen. nov., sp. nov., a mesophilic type I methanotroph isolated from rice rhizosphere, *Int. J. Syst. Evol. Microbiol.* 65 (2015) 3527–3534, <https://doi.org/10.1099/ijsem.0.000451>.
- [49] F. Iannacone, F. Di Capua, F. Granata, R. Gargano, G. Esposito, Simultaneous nitrification, denitrification and phosphorus removal in a continuous-flow moving bed biofilm reactor alternating microaerobic and aerobic conditions, *Bioresour. Technol.* 310 (2020) 123453.
- [50] D. Jiang, M. Curtis, E. Troop, K. Scheible, J. McGrath, B. Hu, S. Suib, D. Raymond, B. Li, A pilot-scale study on utilizing multi-anode/cathode microbial fuel cells (MAC MFCs) to enhance the power production in wastewater treatment, *Int. J. Hydrogen Energy* 36 (2011) 876–884, <https://doi.org/10.1016/j.ijhydene.2010.08.074>.
- [51] H. Hiegemann, D. Herzer, E. Nettmann, M. Lubken, P. Schulte, K. Schmelz, S. Gredigk-Hoffmann, M. Wichern, An integrated 45 L pilot microbial fuel cell system at a full-scale wastewater treatment plant, *Bioresour. Technol.* 218 (2016) 115–122, <https://doi.org/10.1016/j.biortech.2016.06.052>.
- [52] P. Liang, R. Duan, Y. Jiang, X. Zhang, Y. Qiu, X. Huang, One-year operation of 1000-L modularized microbial fuel cell for municipal wastewater treatment, *Water Res.* 141 (2018) 1–8, <https://doi.org/10.1016/j.watres.2018.04.066>.